Journal Pre-proof

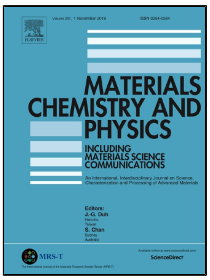

Electrical, morphology and structural properties of biodegradable nanocomposite polyvinyl-acetate/ cellulose nanocrystals

I. Hammami, K. Benhamou, H. Hammami, S. SoretoTeixeira, M. Arous, H. Kaddami, M.P.F. Graça, L.C. Costa

PII:	S0254-0584(19)30998-8
DOI:	https://doi.org/10.1016/j.matchemphys.2019.122182
Article Number:	122182
Reference:	MAC 122182
To appear in:	*Materials Chemistry and Physics*
Received Date:	10 April 2019
Accepted Date:	14 September 2019

Please cite this article as: I. Hammami, K. Benhamou, H. Hammami, S. SoretoTeixeira, M. Arous, H. Kaddami, M.P.F. Graça, L.C. Costa, Electrical, morphology and structural properties of biodegradable nanocomposite polyvinyl-acetate/ cellulose nanocrystals, *Materials Chemistry and Physics* (2019), https://doi.org/10.1016/j.matchemphys.2019.122182

Electrical, morphology and structural properties of biodegradable nanocomposite polyvinyl-acetate/ cellulose nanocrystals

I. Hammami[a*], K. Benhamou[b],H. Hammami[a],S.SoretoTeixeira[c],M. Arous[a],H. Kaddami[b], M.P.F. Graça[c], L.C. Costa[c]

[a]*LaMaCoP, Faculty of Sciences of Sfax, University of Sfax, BP 3018 Sfax, Tunisia*

[b] *Laboratory of Organometallic and Macromolecular Chemistry-Composites Materials, Faculty of Sciences and Technologies, Cadi-Ayyad University, 40000 Marrakech, Morocco*

[c] *I3N and Physics Department, University of Aveiro, Aveiro, Portugal*

*Corresponding author: Tel.: +216 20220850

E-mail address: imen.hammami1992@gmail.com.

ABSTRACT

In this work, the dielectric properties and the electrical conductivity of polyvinyl acetate (PVAc) polymer doped with cellulose nanocrystals (CNC), extracted from the date palm rachis, are reported. We investigate the filler effect on the molecular mobility of the PVAc polymer chains and the charge transport properties of this material. PVAc/CNC films structure was characterized by powder X-Ray diffraction (XRD), showing the crystalline behavior of the cellulose filler. The dielectric properties were investigated using impedance spectroscopy, in the frequency range of 102–106 Hz and temperatures from 200 to 350 K. A β relaxation, assigned to the motions of the -OCOCH3 side groups, and α relaxation, associated with the glass transition of the PVAc matrix, can be detected.

Keywords: nanocomposites; dielectric properties; polyvinyl acetate.

1. Introduction

Since their advent, composites are widely used in everyday life due to their interesting properties. The incorporation of nanometric particles causes the increase of the matrix/reinforcement interface and leads thereafter to the improvement of the different properties of the materials. The most frequently used nanoparticles are non-biodegradable materials derived from petroleum products (carbon black, carbon nanotubes) or minerals (silicate, clays). However, these different fillers have the disadvantage of not being renewable or biodegradable and can have negative impacts on humans and in the environment [1]. To meet the concern of preserving the environment, several efforts and investigations have been carried out by scientists, which aim to incorporate plant-based materials capable of replacing toxic or non-biodegradable ones and offering at least equivalent properties. Many of these investigations are conducted on the use of cellulosic nanofillers [2, 3]. Nanocellulose is a particularly attractive charge and they have been widely used in the electrical application field, as separators in lithium-ion battery [4], electrolyte additives [5] and humidity sensors [6].

Cellulose is a linear homopolymer composed of D-glucopyranose. Because of the hydroxyl groups present on the surface of the cellulose, the formation of hydrogen bonding is favored, and the cellulose chains are assembled into highly ordered structures. Depending on the pretreatment, nanocellulose can be classified into two main categories: cellulose nanocrystals(CNC), and cellulose nanofibrils (CNF). Cellulose nanocrystal was used frequently as nanofiller in polymers based nanocomposites and was proven an excellent charge [7, 8, 9]. Indeed, introducing small amounts of cellulose nano charges into the matrix generates some changes in tensile strength, Young's modulus, dielectric strength and electrical conductivity. The main employed method used to obtain the cellulose nanocrystals is hydrolysis with sulfuric and hydrochloric acid.

Polyvinyl acetate (PVAc) is an amorphous and biodegradable polymer [10]. It has good insulating properties with low conductivity and frequently used in microelectronic applications [11]. The presence of cellulose nanoparticles induces an improvement in its properties and particularly the electrical and mechanical properties [12, 13].

Understanding the dielectric properties of nanocomposite thermoplastic polymers is of great importance in gaining fundamental knowledge for predicting the mechanical properties of these materials. The dielectric relaxation spectroscopy is an effective way of probing the microstructure and assessing the dipoles motions and interactions of the nanocomposites at a different range of frequencies and temperatures.The structure-property relationship of PVAc-based nanocomposites is rarely studied, while most studies have focused on the thermal degradation behavior of pure PVAc [14]. Sternstein and Zhu [15] indicated in their study that the hydroxyl groups on the surface of silica particles could form hydrogen bonds with the PVAc acetate group, which resulted in a significant effect of the reinforcement in the nanocomposites. These results indicate that it may be possible to obtain promising properties for nanocomposites based on PVAc and CNC. That was also illustratedin some pioneering works [16, 17, 18].
In this work, cellulose nanocrystals extracted from the rachis of the date palm tree were used to prepare nanocomposites based on PVAc as a matrix. The use of such filler is justified by its high aspect ratio and by the availability of this natural resource in North Africa [19]. In fact, it is well known that after the fruit harvesting, the date palm trees need to be maintained. Indeed, during the maintenance of the date palm, a large amount of waste is generated. Until now, this waste is used as a source of domestic energy or as a barrier against the silting up of agricultural land in the Sahara regions. The current study is in keeping with the general pattern aiming at the valorization of these plant resources and the exploitation of this abundant natural deposit.
The electrical properties and the ionic conduction mechanism of these nanostructured materials were explored using complex impedance analysis. In fact, the electrical investigation method can gives more informations about the mechanisms of charge transport and interfacial polarization and subsequently the quality of matrix reinforcement adhesion. On the other hand the potential of using these composites as separators for ionic battery might be considered.

2. Experimental Section

2.1. Materials

2.1.1. Polymer matrix

An amorphous thermoplastic polymer, polyvinyl acetate PVAc, with a molecular weight of 207 761 Da, was synthetized and used in this study as matrix material. To synthesis PVAc free radical polymerization of VAc monomer in the presence of benzoyl peroxide as initiator was used. A mixture containing the VAc monomer and 2 wt% of benzoyl peroxide is poured into a three-necked round-bottom flask equipped with a reflux condenser and a mechanical stirrer. The polymerization was conducted at a temperature of 80 °C and under a dry nitrogen atmosphere. After 30 min reaction, when the solution became strongly viscous, it was cooled and solubilized in a minimum of methanol and precipitated in distilled water. The Tg by DSC of the synthesized polymer is 45°C [8], which means that it's partially hydrolysed

2.1.2. Cellulose nanocrystals

Cellulose nanocrystals were prepared according to the method used by Benhamou et al. [8]. Briefly, palm tree rachis were cut into small pieces and ground to powder. The powder is extracted with soxhlet for 24 h, using a mixture of ethanol and toluene, to remove pigments, lipids, waxes and all substances soluble in organic solvents. The pulp is treated with a sodium hydroxide solution (NaOH) for 2 h, at 80 °C, to eliminate hemicelluloses and lignin, followed by treatment by sodium chlorite solution at 70 °C for 2 h, to eliminate remaining lignin. The suspension is filtered, washed extensively with water and the treatment is repeated until complete bleaching of the pulp. Then, the bleached pulp is treated using concentrated sulphuric acid at 45 °C during 45 min to obtain the CNC suspension. The obtained CNC have an average diameter of 5.8 ± 1.5 nm and length about 235 ± 21 nm [7]. The zeta potential of CNC calculated in a previous study of the author was estimated to -56 mV at pH 5-6 [20].

2.1.3. PVA/NCC nanocomposites preparation

In this study, a solvent exchange method was used to transfer CNC from water to methanol. This method enables avoiding CNC drying and insures better re-dispersion in organic solvent. Therefore CNC agglomeration is maintained at its lower level.
The water suspension of CNC was solvent-exchanged to acetone and then to dry methanol (The CNC concentration in these solvents was around 2% in weight) by successive centrifugation and dispersion operations. The PVAc/methanol solution and CNF/methanol dispersion were mixed in different ratios to vary the CNC content in the final nanocomposite from 0 to 10 wt%. Each mixture was stirred for one complete day by magnetic stirring and then by means of the high power ultrasound disperser was sonicated of for 5 min and then degassed. The nanocomposite films were prepared by casting method, each dispersion was poured into a Teflon mold and keept at room temperature for two weeks for slow elimination of methanol. The nanocomposite films were then dried overnight under vacuum at 50 °C.

2.2. Experimental procedure

The morphologies of samples were analyzed by TESCAN–VegaIII scanning electron microscopy (SEM). The specimens were frozen under liquid nitrogen, fractured, mounted, coated with carbon and observed using an applied tension of 40 kV.

X-ray diffraction (XRD) patterns were obtained using a Siemens D5000 diffractometer with mono-chromatic Cu-Kα radiation ((λ=1.54056 Å) over a 2θ range from 2° and 80°, at room temperature.

Impedance spectroscopy measurements were performed using an Agilent 4294A precision impedancemeter, measuring in the Cp–Rp configuration, in the temperature range from 200 K to 350 K with 5 K step and in a broad frequency window from 100 Hz to 1 MHz. For the dielectric analysis, an alternating voltage with amplitude 1 V was applied to a sample placed between two parallel plate electrodes.
The dielectric behavior is investigated with the complex dielectric constant ε^* expressed as [21]:

$$\varepsilon^* = \varepsilon' - j\varepsilon'' \tag{1}$$

The alternative current (AC) conductivity has been determined from the dielectric losses according to the relation:

$$\sigma^* = j\varepsilon_0\omega\varepsilon^*(\omega) = j\varepsilon_0\omega\,(\varepsilon' - j\varepsilon'') = \varepsilon_0\omega\varepsilon'' + j\varepsilon_0\omega\varepsilon' \tag{2}$$

Where ε_0 is the permittivity of the free space and $\omega = 2\pi f$ is the angular frequency.

The direct current (DC) conductivity measurements were carried out using a 617 Keithley electrometer. The samples were prepared in the form of discs of 10 mm diameter. The electrical measurement was done using a two aluminum plate pressure system, where the sample was placed between them. DC voltages (50 V, 100 V) were applied across the thin film. The experiment consists of measuring the electrical resistance of each sample to calculate the DC conductivity for the different series of the composites, at a constant temperature. The electrical conductivity σ_{DC}, at a given temperature,can be determined using the following equation [22, 23]:

$$\sigma_{DC} = \frac{1}{\rho_{DC}} = \frac{L}{R\,.A} \tag{3}$$

Where ρ_{DC} is the resistivity, L is the thickness, A is the electrode cross-sectional area and R is the resistance of the studied sample.

3. Results and discussion

3.1. Morphological analysis

Figure 1 shows SEM images of the freshly fractured surface for PVAc matrix and nanocomposites felt with 1 and 10wt% of CNC.

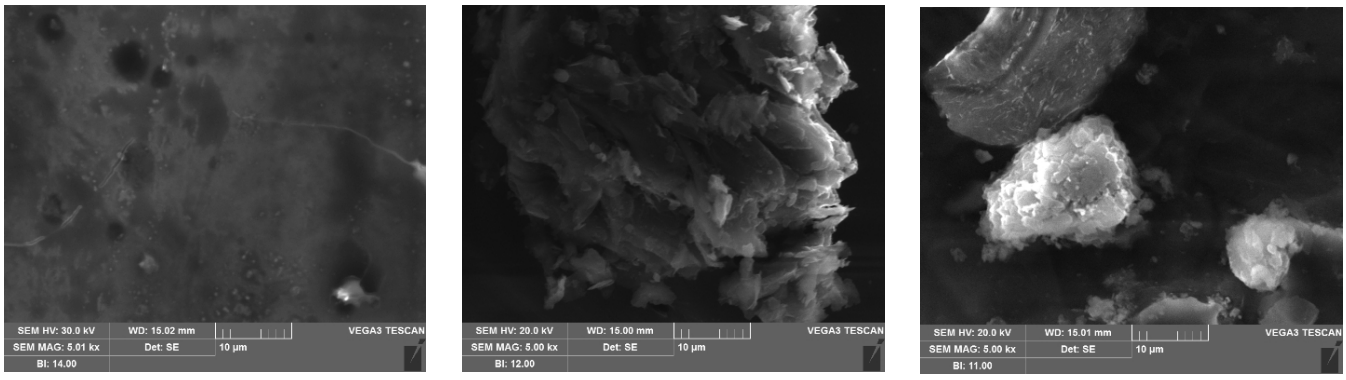

(a) (b) (c)

Figure 1. SEM micrographs of: (a) PVAc matrix; (b) PVAc+1% CNC; (c) PVAc+10% CNC.

The SEM images of pure PVAc (figure 1.a) show the presence of cracks on the surface of the section, accompanied by fissures, while the nanocomposites showed different morphologies. Figures 1.b and 1.c show that, for the nanocomposites, fracture

surface was relatively rougher compared to the pure PVAc sample. Also, the grains observed on the nanocomposite samples can be considered as CNC aggregates. By increasing the CNC content, the amount of these grains was found to increase, indicating that they were mostly dispersed in PVAc matrix. Similar morphologies have been observed for the nanocomposites based on PVAc and TEMPO-CNF (nanofibrillated cellulose obtained via TEMPO mediated oxidation), where the addition of TEMPO-CNF rend the fracture surface rough and aggregates could be observed at high TEMPO-CNF contents [24].

3.2. X-ray Diffraction (XRD)

The structure of the samples was analyzed by XRD and the obtained patterns are shown in figure 2. One can notice the absence of discrete peaks of diffraction on the spectrum of the PVAc, in fact, the large visible bumps are created by distributions of lines related to the disorder in the solid confirming the amorphous structure of this polymer. However, in the case of PVAc filled with 10wt% of CNC, five fine and less fine diffraction peaks could be observed, especially at 22.64° (020 plane) and 34.6° (004 plane) ascribed to cellulose type I [25, 26]. This result can be confirmed by comparing the XRD patterns of PVAc+10% CNC with the those obtained for CNC nanofillers. The other characteristic peaks of cellulose I, which should appear, especially the one at 14.07°, corresponding to 110 plane, is embedded in the bumps of the amorphous PVAc.

(a)

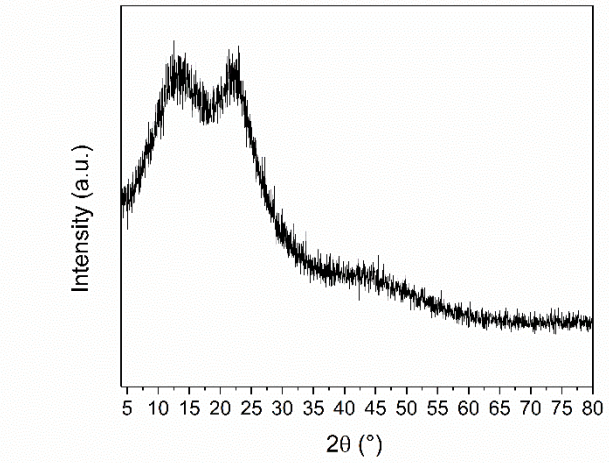

(b)

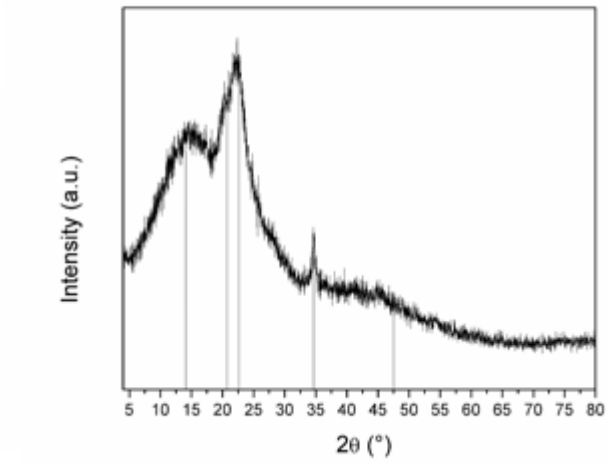

(c)

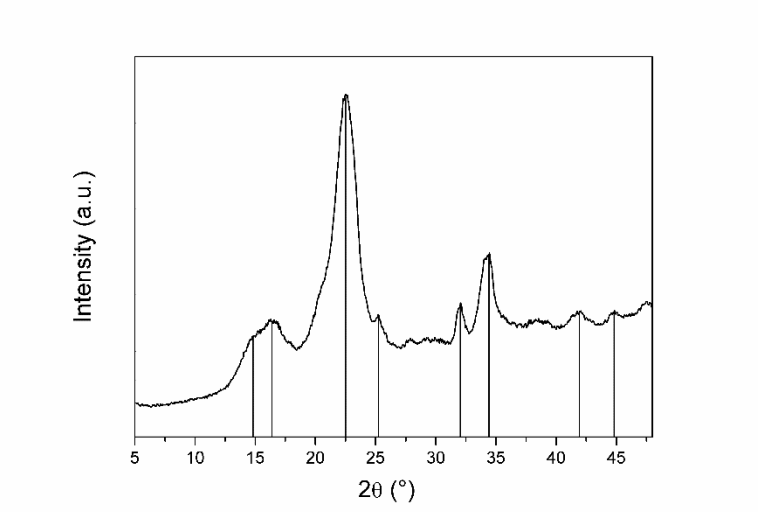

Figure 2. XRD patterns of : (a) PVAc matrix,(b) PVAc+10% CNC nanocomposite and (c) CNC nanofillers.

3.3. Dielectric studies

3.3.1 Polyvinyl acetate matrix

The dependence of the imaginary, ε", part of the complex permittivity versus temperature and frequency and the dependence of the real, ε', and imaginary, ε", parts of the complex permittivity versus frequency at different temperatures for the matrix PVAc are shown in Fig.3a, Fig.3b and Fig.3c respectively

(a)

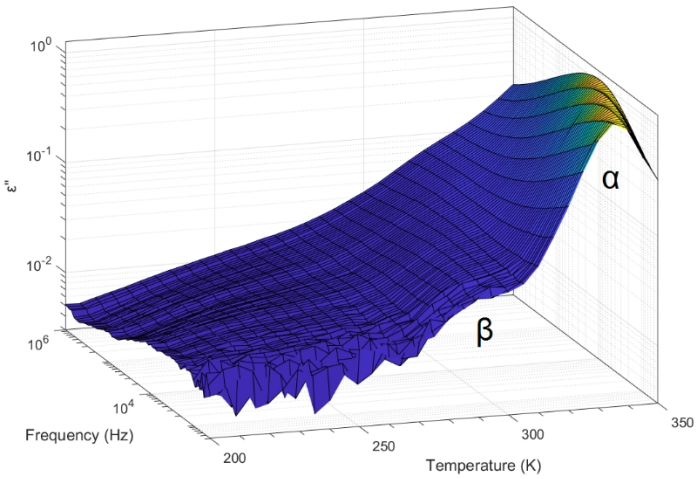

(b)

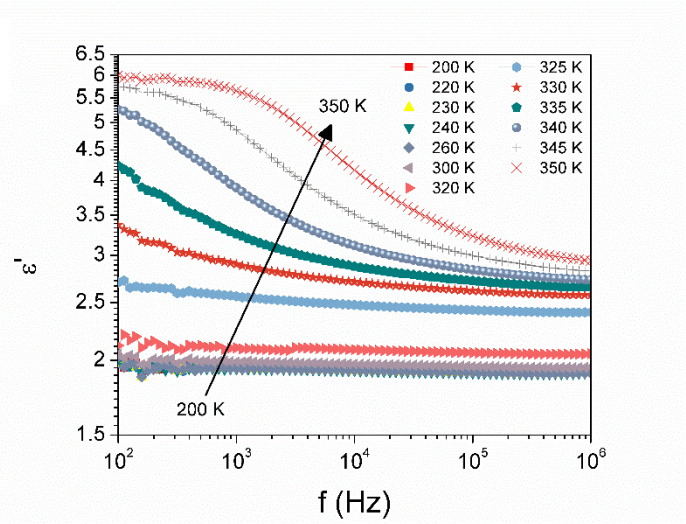

(c)

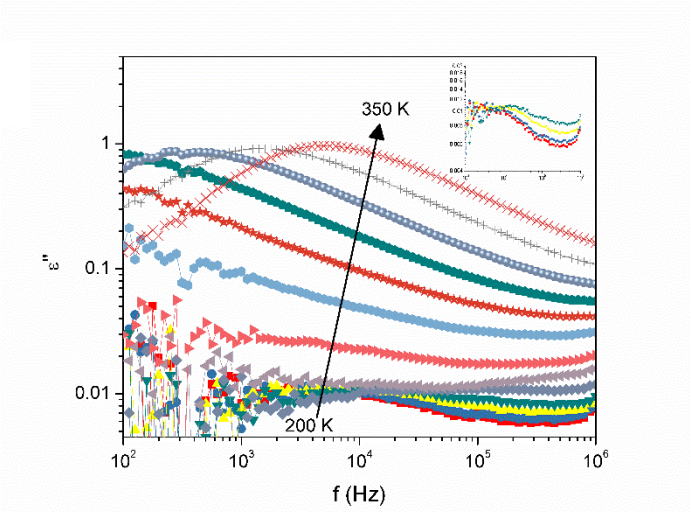

Figure 3. (a) 3D graphs of the imaginary part of the dielectric permittivity versus frequency and temperature for the PVAc matrix; (b) and (c) are respectively the frequency dependence of real and imaginary parts of the dielectric permittivity for the PVAc matrix. The inset shows enlarged β-relaxation region.

Two relaxation modes are observed:

i. The primary relaxation, α-relaxation, appearing at temperatures above 330 K. It is associated with the glass–rubbery transition of the PVAc matrix. This relaxation peak is shifted to higher frequencies when the temperature increases, due to the faster molecule movements leading to the decrease in the relaxation times [27].
ii. The secondary relaxation, β-relaxation, which is observed in the temperature range 200 K and 250 K. This relaxation is assigned to the motions of the -OCOCH3 side groups [28].

3.3.2 Nanocomposites

(a)

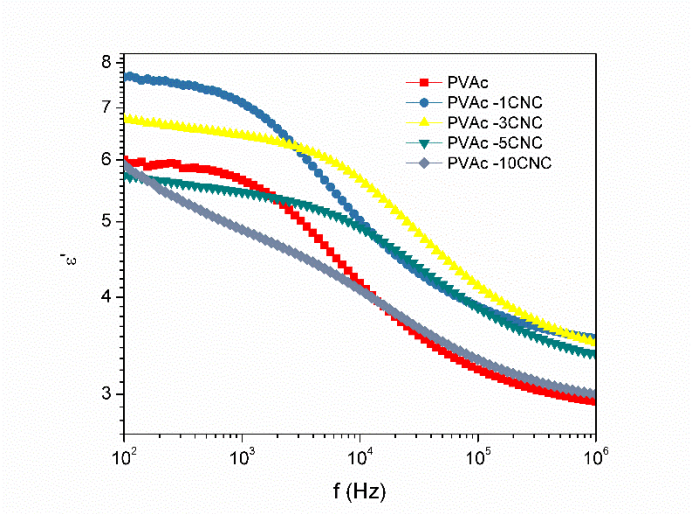

(b)

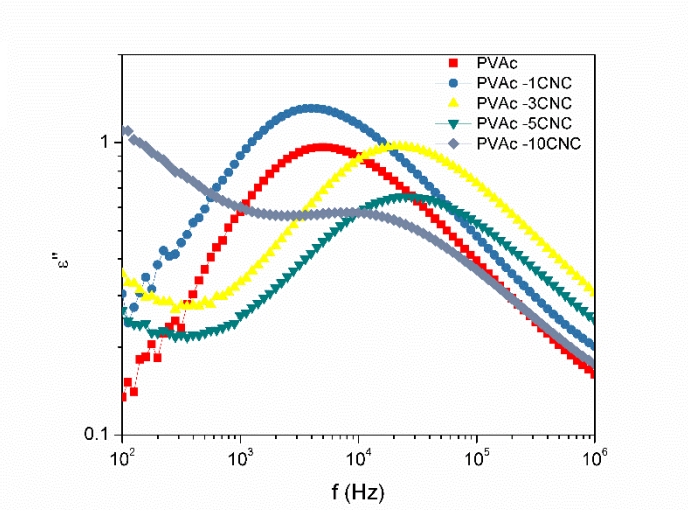

Figure 4. Frequency dependence of (a) real part, ε', and (b) imaginary part, ε", of the dielectric permittivity for the PVAc matrix and PVAc/CNC nanocomposites, at 350 K.

The real and the imaginary parts of the complex permittivity, as a function of frequency, are shown in figure 4.
The incorporation of filler into a polymer matrix induces changes in the properties of the resulting composite. The interactions between the inclusions and the polymer matrix affect the glass transition temperature. If these interactions are attractive, the polymer chains are restricted by the inclusions, and the movement of the macromolecular chains becomes slower. Thereby, T_g increases and the process is specified by a longer relaxation time and therefore observed at lower frequencies. The opposite occurs when the matrix-charge interactions are repulsive; as the motion of the macromolecules becomes easier, Tg decreases, the relaxation time of the process becomes shorter, and the relevant loss peak is observed at higher frequencies [29].
From figure 4, we notice a slight shifting in the loss peak position of the PVAc-1%CNC nanocomposite to lower frequencies compared to the corresponding one of the neat PVAc. This indicates that the interactions between the CNC nanoparticles and the PVAc matrix are attractive. The increase in the percentage of filler causes the shifting of loss peak maxima to higher frequencies, indicating an appreciable reduction of attractive forces or even a switch to repulsive interactions. The attractive interaction for the PVAc-1%CNC nanocomposite is may be due to few physical cross links that developed between the PVAc matrix (which is partially hydrolyzed) and nanocharge. These physical crosslink take place between the hydroxyl sites of PVAc and CNC, which is considered as emulsifying effect of the hydrolyzed sequences of PVAc. However for higher loading, the CNC-PVAc interaction found to be repulsive (interactions between acetate groups of PVAc and CNC) because all hydroxyl sites are saturated [30, 31].

Furthermore, only for the PVAc-10%CNC nanocomposite, figure 4 shows a linear increase when decreasing frequency of the dielectric constant (ε') and loss factor (ε") at low frequencies, which reveals the presence of an additional process. As it is widely known in polymers, the high increases of the dielectric permittivity ε' and loss factor, ε", at low-frequency ranges and above the glass transition temperature T_g are related to the ionic conduction that appears due to the increase in the electric charges mobility with temperature. However, in this low-frequency range, other phenomena can be detected such as the electrode polarization, related to the accumulation of free charges at the electrode interfaces [32], and the interfacial polarization known as the Maxwell-Wagner-Sillars (MWS), derived from the migration and accumulation of charges carriers at the interfaces between the heterogeneous systems [33]. It is worth to note that the interfacial polarization and electrode polarization are often confounded with ionic conduction, as these phenomena are originated from charged carrier mobility [34].
To further investigate the phenomena that occur at the low frequencies region, we present, in figure 5, the frequency dependence of the AC conductivity for the PVA matrix and the PVA/CNC nanocomposite. In the case of the nanocomposite materials, the conductivity AC obeys the following empirical power law [35, 36]:

$$\sigma_{AC}(\omega) = \sigma_{DC} + B\omega^{s} \tag{4}$$

where σ_{DC} is the frequency independent DC limit of conductivity at $\omega = 0$, B is a constant depending on temperature which reflects the polarizability, and s is the frequency exponent representing the degree of interaction between mobile ions and the surrounding environment [37], varying between 0 and 1.
Based on the equation (4), the variation of the conductivity AC versus the frequency must show two distinct types of behavior. The first behavior appears at high frequencies, where the conductivity is an increasing function of frequency $(\sigma'(\omega) = B\omega^{s})$ following a slope close to the unity ($0.8 \leq s \leq 1$). At lower frequencies, the conductivity usually is independent of the frequency, presenting a horizontal plateau associated with the conductivity deriving from the transport of the long-range ions is appearing, which is not the case in our samples (figure 5). Therefore, the ionic conductivity and the electrode polarization are omitted. This effect could be observed at higher temperatures and lower frequencies.

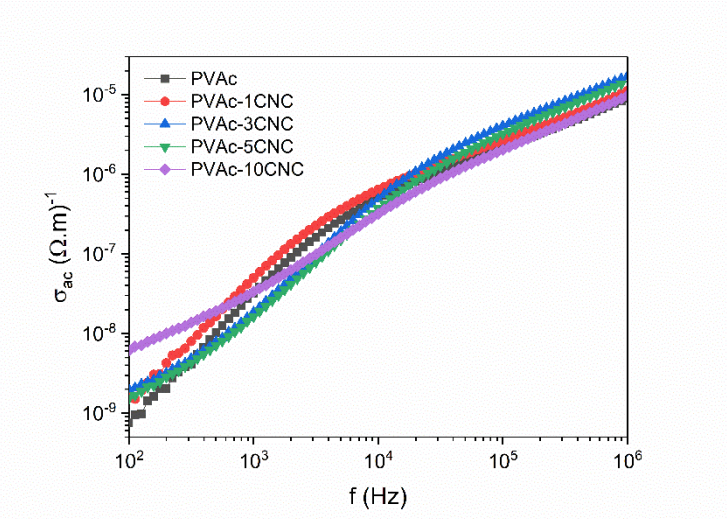

Figure 5. AC conductivity of PVAc matrix ant PVAc/CNC nanocomposites versus frequency at 350 K.

The incorporation of CNC charge leads to the appearance of an additional process at high temperatures and low frequencies, ascribed to MWS interfacial polarization. This relaxation results from the accumulation of charge carriers at the interfaces between the PVA matrix and the CNC nanofillers. It is better defined and appears more intense in the nanocomposite having 10% of charges. Indeed, the more we introduce the nanofiller in the matrix, the more we multiply the interfaces. This can be confirmed by the quasi-inexistence of this relaxation for the nanocomposites having a rate of 1%, 3% and 5% of charges.

3.4. Molecular dynamics

The effect of CNC charges on segmental mobility is further analyzed by performing an analysis based on fitting appropriate model functions. The imaginary part of the permittivity spectra was fitted following the Havriliak-Negami (HN) function:

$$\varepsilon'' = \sum_i \left[\frac{\Delta\varepsilon_i \sin\theta}{\left[1 + 2(\omega\tau_{HN_i})^{\alpha_i}\cos\left(\frac{\alpha_i\pi}{2}\right) + (\omega\tau_{HN_i})^{2\alpha_i}\right]^{\frac{\beta_i}{2}}} \right] + \left(\frac{\sigma_{DC}}{\varepsilon_0\omega}\right)^N \quad (5)$$

With, $\theta = \beta atan\left[\frac{(\omega\tau_{HN})^{\alpha}\sin\left(\frac{\alpha\pi}{2}\right)}{1 + (\omega\tau_{HN})^{\alpha}\cos\left(\frac{\alpha\pi}{2}\right)}\right]$

The index i represent the different relaxations involved in dielectric spectra; Δεi is the relaxation strength values, and τ is the characteristic relaxation time; ($\sigma_{DC}/\varepsilon_0\omega$) is the DC conductivity term; α and β are parameters that respectively related to the broadness and asymmetric of the relaxation times distribution.

As it can be seen in figure 6, α increases with the rise of the temperature indicating a decrease on the broadness of the relaxation time distribution, suggesting that the response of the dipoles to the external electric field becomes more uniform. It also indicates that this parameter is thermal activate. With the composition, it shows that increasing the content of CNC the α value decreases. This should be related with the increase of the number of the dipoles and consequently an increase in the randomness of the relaxation times.

The β parameter increases with temperature and CNC content, showing an approximation to the empirical Cole-Cole model.

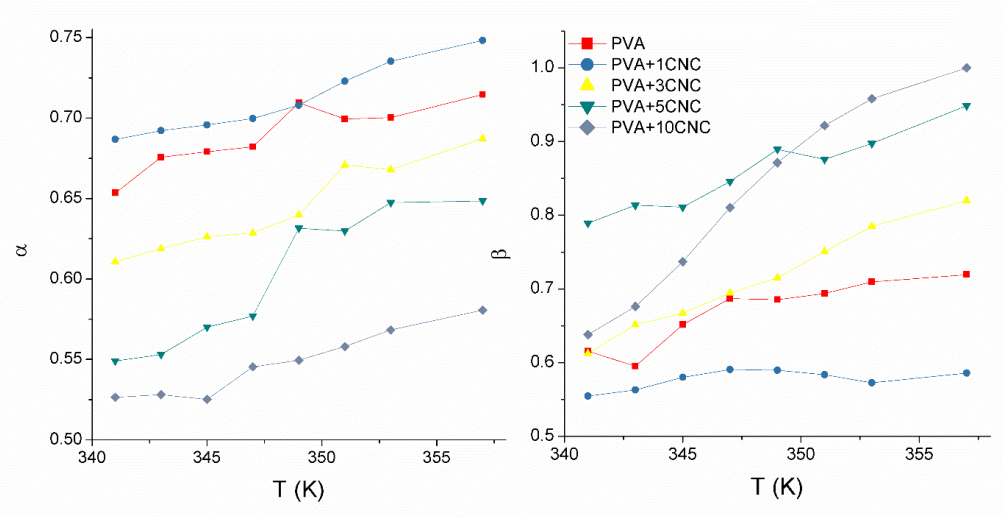

Figure 6. The evolution of the symmetric α and asymmetric β parameters versus temperature for the different PVAc/CNC nanocomposites.

The relaxation times versus the reciprocal of the temperature can be seen in figure 7.

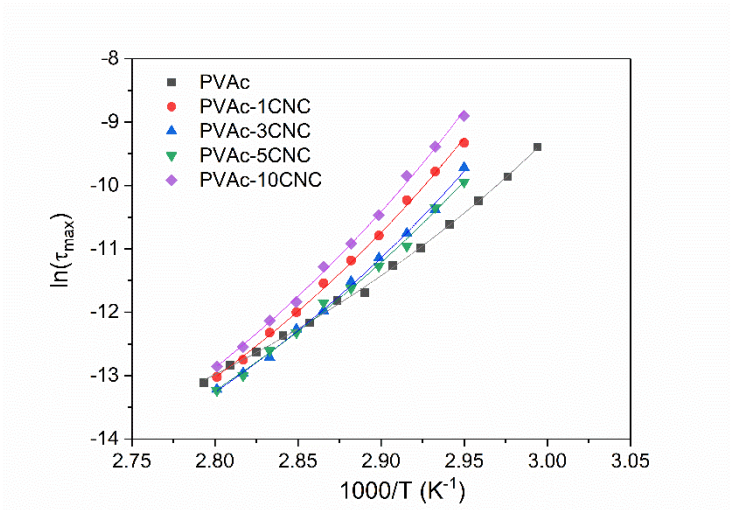

Figure 7.Relaxation map showing the temperature dependence of the relaxation time for the α process. The lines represent the Vogel–Fulcher–Tammann (VFT) fitting result.

The temperature dependence of the relaxation rate for the α –relaxations was better described by the Vogel–Fulcher–Tammann (VFT) equation [38, 39, 40]:

$$\boldsymbol{\tau_{max}(T) = \tau_0 \exp\left(\frac{DT_0}{T - T_0}\right)} \tag{6}$$

Where τ_0 is a pre-exponential factor, T_0 is the Vogel temperature (ideal glass transition), which it was found to lie between 30 and 70 K below glass transition temperature Tg [41]. D, the so-called strength parameter [42], is a measure of the fragility factor describing a deviation of the temperature dependence of τ (T) from the Arrhenius behavior.

The calculated parameters for this relaxation processes are listed in Table 1.
We find that the values of the fragility parameters D for α relaxation increase considerably as a function of reinforcement rate indicating the reinforcing effect of the cellulose nanofiller which limits the mobility of the PVAc chains.

3.5. DC Conductivity studies

3.5.1 Temperature dependent conductivity studies

The temperature dependence of the DC electrical conductivity was studied in the range of 200 K–350 K for all the samples. The following figure displays the conductivity versus 1000/T for PVAc-CNC nanocomposite.

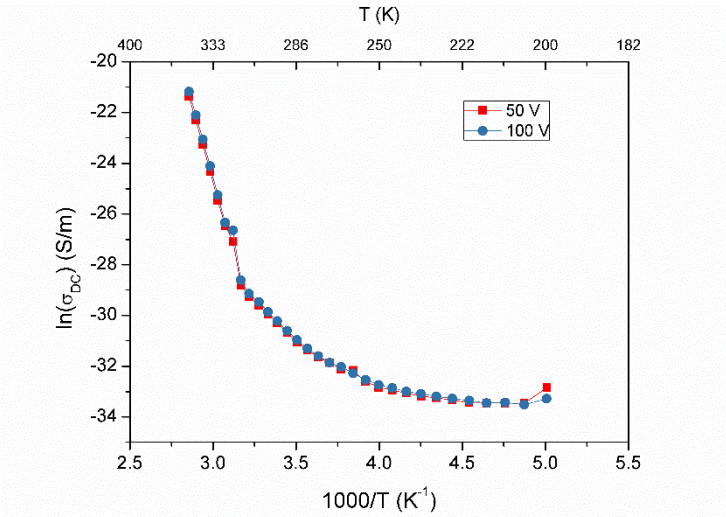

Figure 8. DC conductivity evolution versus 1000/T for PVAc-1%CNC nanocomposite.

As we can see in figure 8, the conductivity is the same for the two applied voltages, corresponding to an ohmic behavior.
Figure 9 shows the DC conductivity versus 1000/T, on a semi-logarithmic scale, for PVAc and PVAc–cellulose nanocomposites. Two distinct conduction regions can be observed: one in the low temperatures range (<250 K) where the σ_{DC} is almost constant and another in the high-temperature measurement range (>250 K) where the σ_{DC} decreases almost linearly with the reciprocal of the temperature.

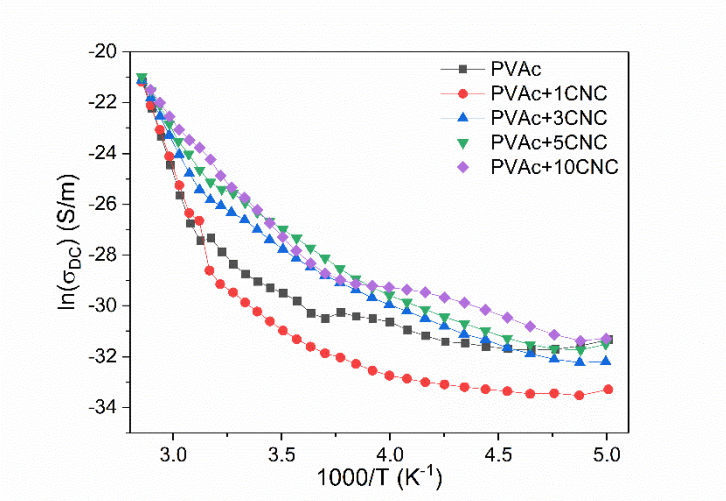

Figure 9. DC conductivity versus 1000/T, on a semi-logarithmic scale, for PVAc and PVAc-CNC nanocompositesat 100 V.

From the slope of the graphs at higher temperatures (T>250K), the activation energy of conduction was estimated using the relation:

$$\boldsymbol{\sigma_{DC} = \sigma_0 \exp\left(\frac{-E_A}{k_B T}\right)} \quad (7)$$

Where σ_0 is the pre-exponential factor, k_B is the Boltzmann's constant, T is the absolute temperature, and E_A is the electrical activation energy under the DC fields. Activation energy values are shown in Table 2.

In general, it is supposed that values of DC activation energy greater than 0.6-0.8 eV would be related to ionic transport and those values less than 0.2 eV should be associated with electronic mechanism [43]. Indeed, the electronic conduction is characterized by high mobilities and low activation energies, while the ionic conduction is associated with relatively lower mobilities and higher activation energies. Therefore, the conduction mechanism, presented in PVAc -CNC films is of ionic nature.
The activation energy decreases with increasing of the filler content. The increase in cellulose nanocrystals means an increase in the heterogeneity of the PVA matrix, which leads to an increase in the resistance of the nanoparticle-polymer interface. Also, the further increase in the CNC nanoparticles concentration results in a decrease in the interseparation distance between the charges or aggregates and then, a physical conductive network for charge carrier transportation has been created in the composite.
Nevertheless, by increasing the CNC nanoparticles introduced in the PVA matrix, a competition of the conductivity enhancement and interfacial polarization leads to the conductivity percolation and minimization of the activation energy.

4. Conclusions

In this study, the morphology, the dielectric and electrical behavior of a series of PVAc matrix charged with different CNC content nanocomposites have been investigated by XRD, SEM and impedance spectroscopy.
The dielectric analyses were carried out to evaluate the CNC content effect on the nanocomposites molecular dynamics and electrical conductivity behavior. The analyzes of the dielectric behavior allowed us to highlight, in the increasing order of temperature, the relaxation β assigned to the motions of the -OCOCH3 side groups and the relaxation α associated with the glass transition of the PVAc matrix.
Also, the temperature dependence of α-relaxation time was modeled by the Vogel–Fulcher–Tammann (VFT) equation. Basing on these data, we found that incorporating CNC lead to a hindrance in the mobility of the PVAc chain, due to attractive interactions between charges and polymer macromolecules.
The analysis of the conductivity is a complementary study of the dielectric properties. Indeed, the decrease of the activation energy with increasing the filler content emphasizes the presence of a conductive network for charge carrier transportation.

References

[1] E. Manaila, M. Stelescu, G. Craciun, Degradation studies realized on natural rubber and plasticized potato starch based eco-composites obtained by peroxide cross-linking, International journal of molecular sciences 19 (10) 40 (2018) 2862.

[2] N. Board, The complete book on biodegradable plastics and polymers (recent developments properties, analyses, materials & processes), Asia Pacific Business Press, Delhi.

[3] W. Den, V. K. Sharma, M. Lee, G. Nadadur, R. S. Varma, Lignocellulosic 45 biomass transformations via greener oxidative pretreatment processes: Access to energy and value-added chemicals, Frontiers in chemistry 6.

[4] Q. Xu, Y.-K. Cheong, S.-Q. He, V. Tiwari, J. Liu, Y. Wang, S. N. Raja, J. Li, Y. Guan, W. Li, Suppression of spinal connexin 43 expression attenuates mechanical hypersensitivity in rats after an l5 spinal nerve injury, 50 Neuroscience letters 566 (2014) 194–199.

[5] A. Chiappone, J. R. Nair, C. Gerbaldi, L. Jabbour, R. Bongiovanni, E. Zeno, D. Beneventi, N. Penazzi, Microfibrillated cellulose as reinforcement for li-ion battery polymer electrolytes with excellent mechanical stability, Journal of Power Sources 196 (23) (2011) 10280–10288.

[6] S. Ummartyotin, H. Manuspiya, A critical review on cellulose: from fundamental to an approach on sensor technology, Renewable and Sustainable Energy Reviews 41 (2015) 402–412.

[7] A. Ladhar, M. Arous, H. Kaddami, M. Raihane, A. Kallel, M. Gra¸ca, L. Costa, Molecular dynamics of nanocomposites natural rubber/cellulose 60 nanowhiskers investigated by impedance spectroscopy, Journal of Molecular Liquids 196 (2014) 187–191.

[8] K. Benhamou, H. Kaddami, A. Magnin, A. Dufresne, A. Ahmad, Biobased polyurethane reinforced with cellulose nanofibers: a comprehensive investigation on the effect of interface, Carbohydrate polymers 122 (2015) 65 202–211.

[9] H.-Y. Yu, Z.-Y. Qin, Surface grafting of cellulose nanocrystals with poly (3-hydroxybutyrate-co-3-hydroxyvalerate), Carbohydrate polymers 101 (2014) 471–478.

[10] A. G. Trejo, Fungal degradation of polyvinyl acetate, Ecotoxicology and 70 environmental safety 16 (1) (1988) 25–35.

[11] R. Ahmed, Electrical conductivity and dielectric relaxation study of polyvinyl acetate/poly methyl methacrylate blends, International Journal of Modern Physics B 26 (29) (2012) 1250159.

[12] R. J. Moon, A. Martini, J. Nairn, J. Simonsen, J. Youngblood, Cellulose nanomaterials review: structure, properties and nanocomposites, Chemical Society Reviews 40 (7) (2011) 3941–3994.

[13] N. David, D. Anavi, M. Milanovich, Y. Popowski, L. Frid, E. Amir, Preparation and properties of electro-conductive fabrics based on polypyrrole: covalent vs. non-covalent attachment, in: IOP Conference Series: Materials Science and Engineering, Vol. 254, IOP Publishing, 2017, p. 032002.

[14] B. J. Holland, J. N. Hay, The thermal degradation of poly (vinyl acetate) measured by thermal analysis–fourier transform infrared spectroscopy, 90 Polymer 43 (8) (2002) 2207–2211.

[15] S. Sternstein, A.-J. Zhu, Reinforcement mechanism of nanofilled polymer melts as elucidated by nonlinear viscoelastic behavior, Macromolecules 35 (19) (2002) 7262–7273.

[16] N.L.G. de Rodriguez, W. Thielemans, A. Dufresne, Sisal cellulose whiskersreinforcedpolyvinylacetatenanocomposites, Cellulose 13 (3) (2006) 261-270.

[17] A. Kaboorani, B.Riedl, P. Blanchet, M. Fellin, O. Hosseinaei, S. Wang, Nanocrystalline cellulose (NCC): A renewable nano-material for polyvinylacetate (PVA) adhesive, EuropeanPolymer Journal 48 (11) (2012) 1829-1837.

[18] J. Sapkota, S. Kumar, C. Weder, E. J.Foster, Influence of processing conditions on properties of poly (vinyl acetate)/cellulose nanocrystal nanocomposites, Macromolecular Materials and Engineering 300 (5) (2015) 562-571.

[19] A. Bendahou, Y. Habibi, H. Kaddami, A. Dufresne, Physico-chemical characterization of palm from phoenix dactylifera–L, preparation of cellulose whiskers and natural rubber–based nanocomposites. Journal of Biobased Materials and Bioenergy 3(1) (2009) 81-90.

[20] B. Seantier, D. Bendahoua, A. Bendahou, Y. Grohens, H. Kaddami, Multi-scale cellulose based new bio-aerogel composites with thermalsuper-insulating and tunable mechanical properties, Carbohydrate Polymers 138 (2016), 335–348.

[21] A. K. Jonscher, Dielectric relaxation in solids, Journal of Physics D: Ap95 plied Physics 32 (14) (1999) R57.

[22] W. D. Callister, Materials science and engineering-an introduction, John wiley& sons, 2007.

[23] G. T. Meaden, Electrical resistance of metals, Springer, 2013.

[24] K. B. Hamou, H. Kaddami, A. Dufresne, S. Boufi, A. Magnin, F. Erchiqui, 100 Impact of tempo-oxidization strength on the properties of cellulose nanofibril reinforced polyvinyl acetate nanocomposites, Carbohydrate polymers 181 (2018) 1061–1070.

[25] M. Wada, L. Heux, J. Sugiyama, Polymorphism of cellulose i family: reinvestigation of cellulose ivi, Biomacromolecules 5 (4) (2004) 1385–1391.

[26] P. Lu, Y.-L. Hsieh, Cellulose isolation and core–shell nanostructures of cellulose nanocrystals from chardonnay grape skins, Carbohydrate Polymers 87 (4) (2012) 2546–2553.

[27] G. Tsangaris, G. Psarras, A. Kontopoulos, Dielectric permittivity and loss of an aluminum-filled epoxy resin, Journal of non-crystalline solids 131 110 (1991) 1164–1168.

[28] D. Fragiadakis, J. Runt, Microstructure and dynamics of semicrystalline poly (ethylene oxide)- poly (vinyl acetate) blends, Macromolecules 43 (2) (2009) 1028–1034.

[29] O. Vryonis, D. Anastassopoulos, A. Vradis, G. Psarras, Dielectric re115 sponse and molecular dynamics in epoxy-basrtio3 nanocomposites: Effect of nanofiller loading, Polymer 95 (2016) 82–90.

[30] S. Singha, M. J. Thomas, Dielectric properties of epoxy nanocomposites, IEEE Transactions on Dielectrics and Electrical Insulation 15 (1) (2008) 12-23.

[31] B. J. Ash, R. W. Siegel, L. S. Schadler, Glass-transition temperature behavior of alumina/PMMA nanocomposites, Journal of Polymer Science Part B: Polymer Physics 42 (23) (2004) 4371-4383.

[32] P. Gonon, T. P. Hong, O. Lesaint, S. Bourdelais, H. Debruyne, Influence of high levels of water absorption on the resistivity and dielectric permittivity of epoxy composites, Polymer testing 24 (6) (2005) 799–804.

[33] M. Samet, V. Levchenko, G. Boiteux, G. Seytre, A. Kallel, A. Serghei, Electrode polarization vs. maxwell-wagner-sillars interfacial polarization in dielectric spectra of materials: Characteristic frequencies and scaling laws, The Journal of chemical physics 142 (19) (2015) 194703.

[34] M. Arous, I. B. Amor, S. Boufi, A. Kallel, Experimental study on dielectric 125 relaxation in alfa fiber reinforced epoxy composites, Journal of applied polymer science 106 (6) (2007) 3631–3640.

[35] M. Pollak, T. Geballe, Low-frequency conductivity due to hopping processes in silicon, Physical Review 122 (6) (1961) 1742.

[36] H. Namikawa, Characterization of the diffusion process in oxide glasses 130 based on the correlation between electric conduction and dielectric relaxation, Journal of Non-Crystalline Solids 18 (2) (1975) 173–195.

[37] R. Chen, L.-F. Chen, C.-T. Chia, Impedance spectroscopic studies on congruent linbo3 single crystal, Journal of Physics: Condensed Matter 19 (8) (2007) 086225.

[38] H. Vogel, The law of the relation between the viscosity of liquids and the temperature, Phys. Z 22 (1921) 645–646. [34] G. S. Fulcher, Analysis of recent measurements of the viscosity of glasses, Journal of the American Ceramic Society 8 (6) (1925) 339–355.

[39] G. S. Fulcher, Analysis of recent measurements of the viscosity of glasses, Journal of the American Ceramic Society 8 (6) (1925) 339–355

[40] G. Tammann, W. Hesse, Die abh¨angigkeit der viscosit¨at von der temperatur 140 bieunterk¨uhltenfl¨ussigkeiten, Zeitschriftf¨uranorganische und allgemeineChemie 156 (1) (1926) 245–257.

[41] F. Kremer, A. Sch¨onhals, Broadband dielectric spectroscopy, 2003.

[42] C. A. Angell, K. L. Ngai, G. B. McKenna, P. F. McMillan, S. W. Martin, Relaxation in glassforming liquids and amorphous solids, Journal of applied 145 physics 88 (6) (2000) 3113–3157.

[43] V. Jain, C. Gupta, R. Jain, Effect of dopant on the electrical conductivity of pva thin films, Indian J. Pure and Appl. Phys 16 (1978) 625.

Figure Captions

Figure 1. SEM micrographs of: (a) PVAc matrix; (b) PVAc+1% CNC; (c) PVAc+10% CNC.

Figure 2. XRD patterns of : (a) PVAc matrix (b) PVAc+10% CNC nanocomposite and (c) CNC nanofillers.

Figure 3. (a) 3D graphs of the imaginary part of the dielectric permittivity versus frequency and temperature for the PVAc matrix; (b) and (c) are respectively the frequency dependence of real and imaginary parts of the dielectric permittivity for the PVAc matrix. The inset shows enlarged β-relaxation region.

Figure 4. Frequency dependence of (a) real part, ε', and (b) imaginary part, ε", of the dielectric permittivity for the PVAc matrix and PVAc/CNC nanocomposites, at 350 K.

Figure 5. AC conductivity of PVAc matrix ant PVAc/CNC nanocomposites versus frequency at 350 K.

Figure 6.The evolution of the symmetric α and asymmetric β parameters versus temperature for the different PVAc/CNC nanocomposites.

Figure 7. Relaxation map showing the temperature dependence of the relaxation time for the α process. The lines represent the Vogel–Fulcher–Tammann (VFT) fitting result.

Figure 8. DC conductivity evolution versus 1000/T for PVAc-1%CNC nanocomposite.

Figure 9. DC conductivity versus 1000/T, on a semi-logarithmic scale, for PVAc and PVAc-CNC nanocomposites at 100 V.

Tables

	Sample	***D***	***T_o (K)***
α	PVAc	1.942	284
Relaxation	PVAc-1CNC	2.292	290
	PVAc-3CNC	2.308	288
	PVAc-5CNC	2.534	284
	PVAc-10CNC	2.603	289

Table 1:Calculated strength parameter D for PVAc/CNC.

Sample	***$\Delta(Ea)_{DC}$ (eV)***
PVAc	2.09
PVAc-1CNC	1.97
PVAc-3CNC	1.33
PVAc-5CNC	1.08
PVAc-10CNC	0.85

Table 2: Calculated activation energy of PVAc and PVAc-CNC nanocomposites.

Electrical, morphology and structural properties of biodegradable nanocomposite polyvinyl-acetate/ cellulose nanocrystals

I. Hammami[a*], K. Benhamou[b], H. Hammami[a], S. Soreto Teixeira[c], M. Arous[a], H. Kaddami[b], M.P.F. Graça[c], L.C. Costa[c]

[a] *LaMaCoP, Faculty of Sciences of Sfax, University of Sfax, BP 3018 Sfax, Tunisia*

[b] *Laboratory of Organometallic and Macromolecular Chemistry-Composites Materials, Faculty of Sciences and Technologies, Cadi-Ayyad University, 40000 Marrakech, Morocco*

[c] *I3N and Physics Department, University of Aveiro, Aveiro, Portugal*

*Corresponding author: Tel.: +216 20220850

E-mail address: imen.hammami1992@gmail.com.

Highlights

- polyvinyl-acetate/cellulose nanocrystals nanocomposites are investigated.
- The fragility parameters and activated energy for different process are evaluated.
- Electrical conductivity are investigated using DC measurements
- High activation energy values prove that the conductivity is of an ionic nature.

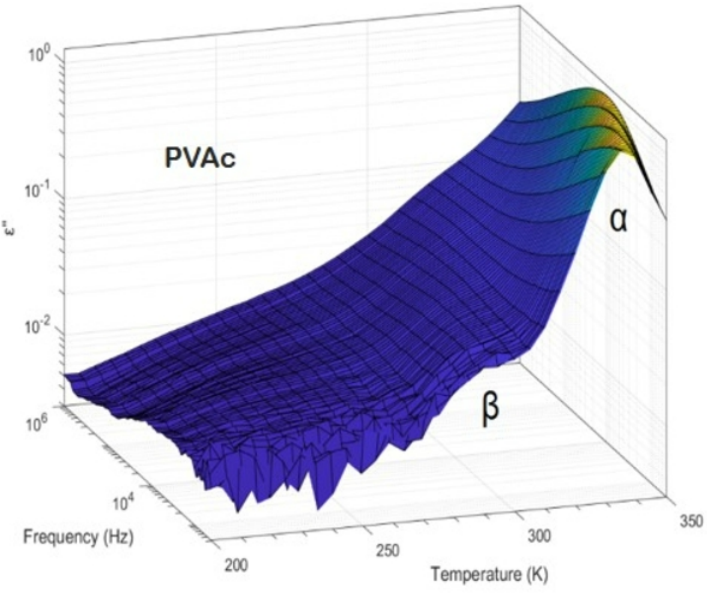
PVAc
α
β
ε''
10^0
10^{-1}
10^{-2}
10^6
10^4
Frequency (Hz)
200
250
300
350
Temperature (K)

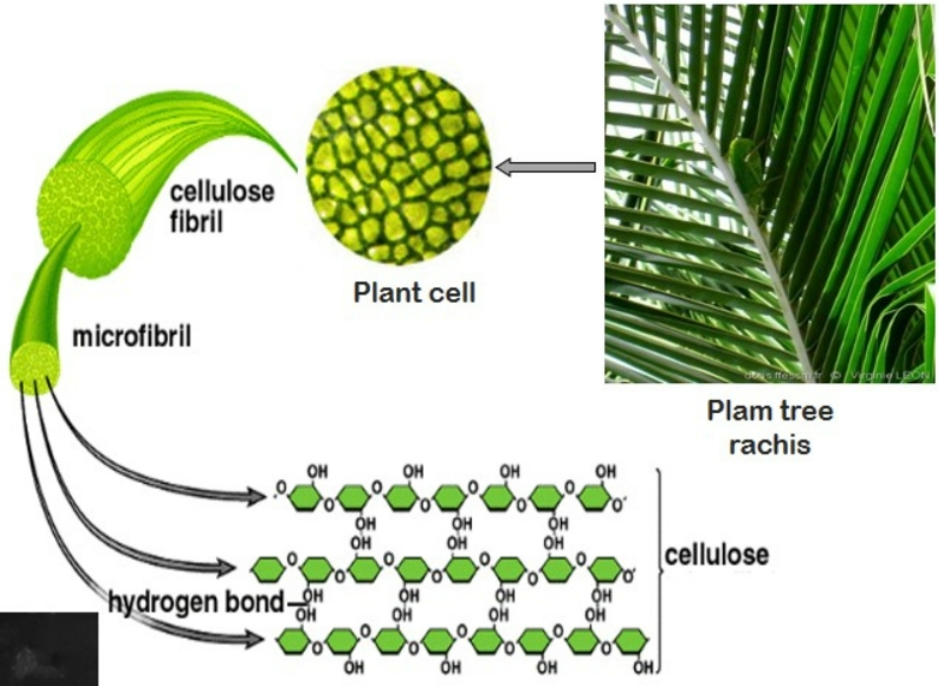
cellulose fibril
Plant cell
microfibril
Plam tree rachis
hydrogen bond
cellulose
OH
O

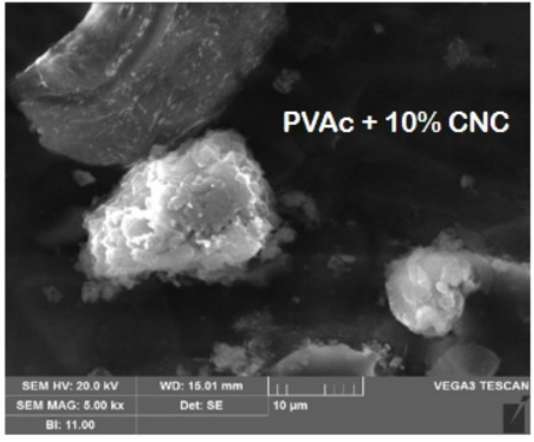
PVAc + 10% CNC
SEM HV: 20.0 kV
WD: 15.01 mm
VEGA3 TESCAN
SEM MAG: 5.00 kx
Det: SE
10 µm
BI: 11.00